# Positron annihilation spectroscopy investigation of vacancy clusters in silicon carbide: Combining experiments and electronic structure calculations

Julia Wiktor,[1,*] Xavier Kerbiriou,[2] Gérald Jomard,[1] Stéphane Esnouf,[3] Marie-France Barthe,[2] and Marjorie Bertolus[1]

[1]*CEA, DEN, DEC, Centre de Cadarache, 13108 Saint-Paul-lez-Durance, France*

[2]*CNRS/CEMHTI, CNRS UPR 3079/CEMHTI, 45071 Orléans, France*

[3]*Laboratoire des Solides Irradiés, École Polytechnique, CEA-IRAMIS, CNRS, 91128 Palaiseau Cedex, France*

The temperature dependence of the point defects in $6H$-SiC induced by 12-MeV proton irradiation was studied by means of isochronal annealing followed by both positron annihilation spectroscopy and electron paramagnetic resonance measurements. The formation energies and positron lifetimes of various vacancy clusters were calculated to help in the interpretation of the experiments. The combination of the experiments and calculations enabled the identification of a negative silicon vacancy, with the lifetime of 218 ps, which is annealed between 400 °C and 700 °C. This process involves vacancy migration and formation of the $V_C + V_{Si}$ cluster, with a lifetime of 235 ps. In addition, our calculations confirm the identification of several clusters proposed in previous experimental studies.

## I. INTRODUCTION

As a wide-band-gap semiconductor, silicon carbide (SiC) has attracted significant attention as a candidate material for high-temperature, high-power, and high-frequency electronic devices. Due to its high thermal conductivity, high-temperature stability, chemical inertness, and small neutron capture cross section, SiC has also potential uses in nuclear applications [1,2]. This material has been proposed for the encapsulation of fissile fuel in high-temperature nuclear reactors [1]. In both electronic and nuclear applications, it is of first importance to know the behavior of this material under irradiation or implantation and studies are still needed to determine fundamental data on the irradiation effects in this material.

Irradiation and implantation creates vacancy-type defects in materials. The vacancies in SiC tend to cluster, as has been shown by the negative binding energies of vacancy clusters calculated theoretically [3] and through appearance of long-lifetime components in positron annihilation spectroscopy experiments [4]. Silicon carbide occurs in many different polytypes, among which $3C$, $4H$, and $6H$ are the most common. Therefore, the defects in these polytypes are most studied, both theoretically [3,5–11] and experimentally, e.g., in positron annihilation spectroscopy (PAS) [4,12–18] or electron paramagnetic resonance (EPR) [19–26].

Positron annihilation spectroscopy is a nondestructive experimental technique allowing one to study open volume defects and is, therefore, an effective method to study vacancies created by irradiation. Vacancies can trap positrons, what is seen through, e.g., changes in positron lifetimes. However, to identify types of the defects present in examined materials, comparison with calculated positron lifetimes or with results of other characterization techniques is required. One of the experimental methods that can facilitate the PAS measurements interpretation is electron paramagnetic resonance (EPR).

Positron lifetimes can be calculated in the two-component density functional theory (TCDFT) [27], which is a

modification of the density functional theory (DFT). The results of our previous theoretical study on monovacancies [28] showed that in positron lifetime calculations in SiC, the full relaxation of defects has to be taken into account. It has also been shown for other semiconductors [29–32]. Thus, a similar study on vacancy complexes is necessary. Additionally, that study showed that the charge states of defects in $6H$-SiC can be predicted by extrapolating the results obtained in $3C$-SiC. Moreover, for the silicon vacancy, the differences in positron lifetimes are very similar in the two polytypes, while for the carbon vacancy the differences are larger. This is why the positron lifetimes of the vacancy complexes need to be compared in $3C$-SiC and $6H$-SiC.

This paper is organized as follows. In Sec. II, we describe the details of the EPR and PAS experiments that were carried out on irradiated $6H$-SiC. In Sec. III, we briefly present the methods used in the calculations of positron lifetimes and defects formation energies and we list the computational details. In Secs. IV and V, we present the results of the experimental studies performed for various measurement and annealing temperatures. In Sec. VI, we present the results of the calculations of the charge states of the vacancy complexes in $3C$-SiC, as well as the positron lifetimes in the two polytypes. Finally, in Sec. VII, we discuss and interpret the experimental results in view of the calculated lifetimes, and in Sec. VIII we compare the calculated results with experimental lifetimes reported in the literature.

## II. EXPERIMENTAL DETAILS

### A. 12-MeV H$^+$ irradiation of 6$H$-SiC crystals and annealing

The $6H$-SiC samples were cut from a low-nitrogen-doped single-crystal wafer ($n_D - n_A = 1.9 \times 10^{17}$ cm$^{-3}$, 385-$\mu$m thick). It was a commercial CREE research (0001)-oriented $6H$-SiC wafer grown using the modified Lely method. The characterization using positron annihilation spectroscopy of the as-received crystals has already been reported [17]. It shows that these samples contain negatively charged nonvacancy defects.

*julia.wiktor@cea.fr

Proton irradiation was performed at room temperature at the CEMHTI Laboratory (Orléans, France) using a cyclotron. The crystals were irradiated under vacuum with 12-MeV protons at a fluence of $4 \times 10^{16}$ cm$^{-2}$ on a water-cooled sample support. The maximum flux used during irradiation was maintained close to $2 \times 10^{13}$ H$^+$ cm$^{-2}$ s$^{-1}$ in order to avoid sample warming. SRIM [33] calculations reported in Ref. [17] showed that 12-MeV protons go through the whole crystal and that the vacancy defects distribution is almost homogeneous as a function of depth. The isochronal annealing [20 min, from 100 °C (EPR study) or 300 °C (PAS study) up to 1050 °C by 50 °C steps] was performed in a rapid thermal annealing furnace under argon atmosphere. Both PAS and EPR spectra were recorded as a function of the sample temperature before annealing and after the various annealing steps.

### B. *X*-band electronic paramagnetic resonance (EPR) measurements

The EPR measurements were performed using an EMX BRUKER spectrometer at 80 and 300 K. This technique allows one to probe unpaired electron defects in solids by measuring the energy absorbed by the material due to electronic transitions. The spectra were decomposed into different Lorentzian-type components using numerical simulation. The spin numbers in the irradiated crystals were determined by comparison with a CuSO$_4$ standard sample measured at the same time. The absorption intensity measured in the sample and the standard sample have been determined by fitting the signal with a sum of Lorentzian functions. The number of spin in the sample is therefore given by the relation as follows:

$$[\text{Spin}]_{\text{sample}} = \frac{3}{4S(S+1)} \frac{I_{\text{sample}}}{I_{\text{standard}}} \frac{\rho}{m} N_{\text{standard}}, \quad (1)$$

where $\rho$ is the volumic mass of the sample, $m$ its weight, $N_{\text{standard}}$ the number of spin centers in the standard sample, $I_{\text{sample}}$ and $I_{\text{standard}}$ the EPR signal intensity in the sample and in the standard sample, respectively. $S$ is the spin of the centers detected in the sample. The defect concentrations given in the following are average values on the whole crystal volume. The spectra are described by the parameters of the Hamiltonian as follows:

$$\mathcal{H} = \mu_{\mathbf{B}} \mathbf{B} \cdot \mathbf{g} \cdot \mathbf{S} + \mathbf{S} \cdot D \cdot \mathbf{S} + \sum_j A_j \mathbf{S} \cdot \mathbf{I}_j \quad (2)$$

with $\mu_{\mathbf{B}}$ the Bohr magneton, $\mathbf{B}$ the magnetic field, $\mathbf{S}$ the effective spin of the defect, $\mathbf{g}$ the $g$ tensor, $D$ the zero-field splitting (ZFS), $A_j$ the hyperfine (HF) interaction constant with the nuclear spin of the neighbor atom $j$, and $\mathbf{I}_j$ the nuclear spin of the neighbor atom $j$. In Sec. IV, we present the first derivative of the EPR spectra for ease of interpretation (Figs. 1 and 2).

### C. Positron lifetime spectroscopy (PAS) measurements

Positron lifetime is the time between the entrance of the positron in the material and its annihilation. Positron annihilation spectroscopy has been described in several publications [32,34,35]. Positrons can be trapped in neutral and negatively charged vacancies or vacancy complexes. They annihilate in these traps with a lifetime $\tau_D$ depending on the defect, which is
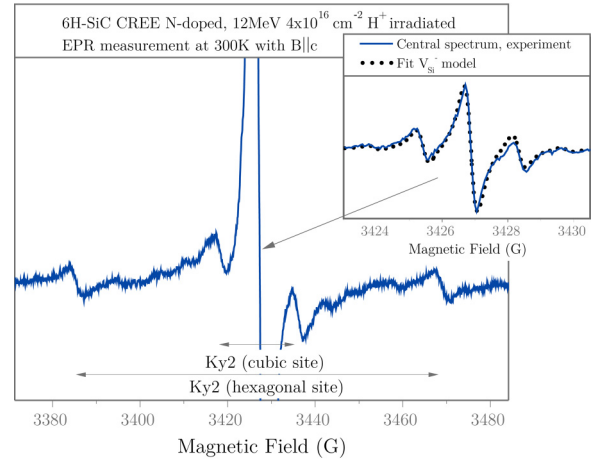


FIG. 1. (Color online) EPR spectrum obtained at 300 K with $B \parallel c$ on the proton as-irradiated 6*H*-SiC CREE crystal. The inset shows the central spectrum and its fit using the $V_{\text{Si}}^{1-}$ model.

longer than the lattice lifetime $\tau_L$, due to the reduced electron density in these defects. Positrons can also be trapped and annihilate in the Rydberg states around negatively charged nonvacancy defects with a lifetime close to $\tau_L$. These traps can either be negatively charged acceptors, antisites, or impurities. They are often called "negative ions." The positron trapping in negative vacancylike defects and around the negative ions decreases as the temperature increases.

PAS measurements were performed using a conventional fast-fast coincidence spectrometer with a time resolution of 230 ps. A $^{22}$Na positron source was sandwiched between two identical samples. The time intervals between the detection of the 1.27-MeV $\beta^+$ decay photon and the 0.511-MeV annihilation photons were measured as a function of the temperature in the 15–575 K range. Approximately two million events were collected for each spectrum. After subtracting the source and background components, the lifetime spectrum is the convolution of the resolution of the spectrometer $R(t)$ with the probability that the positron annihilates at the time $t$, i.e.,
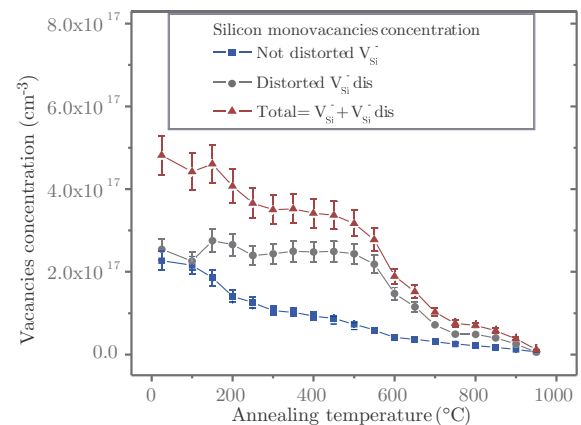


FIG. 2. (Color online) Silicon vacancies concentration (not distorted, distorted, sum) as a function of the annealing temperature in the 6*H*-SiC H$^+$ 12-MeV irradiated crystal.

a sum of decreasing exponentials

$$L(t) = R(t) * \sum_i I_i \exp\left(\frac{-t}{\tau_i}\right). \tag{3}$$

These spectra were fitted with one or two components using a modified version of the POSFIT [36] software. For a two-component decomposition, Eq. (3) becomes

$$L(t) = R(t) * \left[I_1 \exp\left(\frac{-t}{\tau_1}\right) + I_2 \exp\left(\frac{-t}{\tau_2}\right)\right], \tag{4}$$

where $I_1$ and $I_2$ are the intensities ($I_1 + I_2 = 1$), and $\tau_1$ and $\tau_2$ are the lifetime components of the spectra. The average lifetime is calculated as follows:

$$\tau_{av} = (I_1\tau_1 + I_2\tau_2). \tag{5}$$

This lifetime increases when the size and/or the concentration of vacancy defects increases.

## III. COMPUTATIONAL METHODS

### A. Formation energies of defects

Knowledge of the charge states of the defects is helpful in the interpretation of the PAS experimental data. Positive vacancies create a long-range repulsive Coulomb potential, hence have small trapping coefficients and should not be detected by PAS. Neutral and negative vacancies, on the contrary, can be detected and distinguished since the trapping coefficient of the negative vacancies decreases with temperature while it is constant for the neutral defects [37].

To predict the dominating charge states of each vacancy complex, we performed formation energy calculations for defects with charges from $-2$ to $+2$. The approach described in our study on monovacancies [28] was used. We recall it briefly here. We used a formula based on the standard formalism proposed by Zhang and Northrup for GaAs [38] and later adapted to SiC by Zywietz, Furthmüller, and Bechstedt [6]. The formation energy $E_f$ is described by Eq. (9) as follows:

$$E_f(V_X,q) = E_{tot}(V_X,q) - n_C\mu_C - n_{Si}\mu_{Si} + q\mu_e, \tag{6}$$

where $E_{tot}(V_X,q)$ is the total energy of the supercell, $n_C$ and $n_{Si}$ are the numbers of carbon and silicon atoms in the cell, $\mu_C$ and $\mu_{Si}$ are the chemical potentials of the carbon and the silicon atoms in SiC, $q$ is the charge of the supercell, and $\mu_e$ is the electron chemical potential, which is later set to zero for the valence band maximum and varies up to the conduction band minimum.

As the chemical potentials of carbon and silicon atoms in SiC are not known, they must be estimated. We use a conventional approximation for the stoichiometric material, i.e.,

$$\mu_C = \mu_C^{bulk} + \tfrac{1}{2}\Delta H_f(SiC) \tag{7}$$

and

$$\mu_{Si} = \mu_{Si}^{bulk} + \tfrac{1}{2}\Delta H_f(SiC), \tag{8}$$

where $\mu_C^{bulk}$ and $\mu_{Si}^{bulk}$ are the chemical potentials of the C atom in diamond and of the Si atom in bulk silicon, respectively. $\Delta H_f$ is the formation enthalpy, calculated as

$$\Delta H_f(SiC) = \mu_{SiC}^{bulk} - \mu_{Si}^{bulk} - \mu_C^{bulk}, \tag{9}$$

where $\mu_{SiC}^{bulk}$ is the energy per SiC pair in the perfect material. We calculated values of $\Delta H_f$, which we found to be equal to $-0.582$ eV for $3C$-SiC and $-0.579$ eV for $6H$-SiC.

Moreover, since the classical supercell approach fails to provide accurate formation energies for charged supercells, we include corrections in Eq. (6). We use $\frac{2}{3}$ of the Madelung term $\Delta E_{el}(q)$ [39,40], which corrects the electrostatic interaction between the defect and its images and is given as

$$\Delta E_{el} = \frac{\alpha q^2}{2\epsilon_0 L}, \tag{10}$$

where $\alpha$ is the Madelung lattice constant, $\epsilon_0$ is the static dielectric constant, and $L$ is the length of the supercell edge. Additionally, a potential alignment $\Delta V$, calculated as proposed by Taylor and Bruneval [41], is used, with

$$\Delta V = \langle v_{KS}^{bulk}\rangle - \langle v_{KS}^{defect}\rangle, \tag{11}$$

where $\langle v_{KS}^{bulk}\rangle$ and $\langle v_{KS}^{defect}\rangle$ are the average Kohn-Sham potentials calculated for the cell without and with the defect, respectively.

Therefore, the final expression of the vacancy formation energy takes the form

$$\begin{aligned}E_f(V_X,q) = {}& E_{tot}(V_X,q) - n_C\mu_{SiC}^{bulk} \\ & - (n_{Si} - n_C)\big(\mu_{Si}^{bulk} + \tfrac{1}{2}\Delta H_f(SiC)\big) \\ & + q(E_{VBM} + \mu_e + \Delta V) + \tfrac{2}{3}\Delta E_{el}(q), \end{aligned} \tag{12}$$

where $E_{VBM}$ is the energy of the valence band maximum in the perfect cell.

The formation energies of charged defects depend on $\mu_e$. However, DFT is known to fail in predicting the ranges of the electron chemical potential. For instance, the band gaps that we obtained, 1.35 eV for $3C$-SiC and 2.01 eV for $6H$-SiC, are much smaller than the values of 2.36 and 3.0 eV [42] found experimentally, respectively. We vary this value only up to the theoretical band-gap edge to be consistent with the method used. Our $\mu_e$ can hence not be directly compared with the experimental one. Additionally, no perfect way of overcoming the consequences of the finite supercell size nor the too small band gap yielded by DFT is known. Thus, the calculated formation energies, especially for the charged defects, should be used qualitatively.

### B. Positron lifetime calculations

To calculate the positron lifetime, it is necessary to know the distributions of both the positron density $n^+(\mathbf{r})$ and the electron density $n(\mathbf{r})$ in the system, as they determine the probability of annihilation. The positron lifetime $\tau$ depends on this probability and can be calculated as the inverse of a trapping rate $\lambda$:

$$\frac{1}{\tau} = \lambda = \pi c r_0^2 \int_{\mathbb{R}^3} d^3\mathbf{r}\, n^+(\mathbf{r})n(\mathbf{r})g(n^+,n), \tag{13}$$

where $c$ is the speed of light and $r_0$ is the classical radius of an electron. The $g(n^+,n)$ term is an enhancement factor taking into account an increase in the electron density at the positron site caused by the screening of this particle by electrons.

The positron and electron densities can be calculated in self-consistent steps, in the two-component density functional

theory (TCDFT) [27]. Several calculation schemes involving different parametrizations and approximations exist [43–45] and we chose to use the one based on the Boroński and Nieminen [44] calculation method, with a parametrization by Puska, Seitsonen, and Nieminen (PSN) [45]. We showed in the case of monovacancies [28] that this method yields satisfactory results for silicon carbide. For the electron-positron correlation functional, we use the same form as in Ref. [45], while for the enhancement factor, we use the form which takes into account the imperfect screening of the positron by electrons in a semiconductor, as was described in the Appendix in Ref. [28]. To take into account the full relaxation of defects, after a full PSN calculation, the forces on the atoms due to the positron, the electrons, and the other nuclei were calculated using the Hellman-Feynman theorem. Ions were moved according to these forces and the procedure was repeated until all forces could be neglected.

### C. Computational details

All calculations presented here were performed in the projector augmented-wave (PAW) formalism [46] using the ABINIT [47–49] code. The PAW data were generated using the ATOMPAW code [50]. The parameters used in the formation energy calculations are presented in Table I, while the parameters used in positron lifetime calculations are given in Table II. These sets of parameters were sufficient to obtain the structures converged to less than $10^{-3}$ Å and the energies to less than 2 meV per atom. Table I also lists the parameters needed for the electrostatic correction in Eq. (10). We permitted a full defect relaxation without conservation of the initial point symmetry, at constant volume (the theoretical equilibrium volume). In the formation energy calculations, we considered the spin polarization. For the atomic relaxation, we used the Broyden-Fletcher-Goldfarb-Shanno minimization scheme (BFGS) [51–54]. Relaxation was stopped when the forces acting on atoms were smaller than 0.005 eV/Å.

In our study on positron lifetimes in $3C$-SiC, we use supercells with 216 atomic sites ($3 \times 3 \times 3$ repetitions of the conventional cell). To verify if this cell is large enough, we compared the results obtained for the longest defect considered, the chain hexavacancy (see Sec. VI B 1), in 64-,

TABLE I. Parameters used in the calculations of the formation energies of charged defects in the $3C$-SiC. The Madelung constant for zinc-blende was taken.

| Formation energies | |
| --- | --- |
| Polytype | $3C$-SiC |
| e-e x-c functional | GGA-PBE [55] |
| Atomic sites | 216 |
| $E_{cut}$ | 700 eV |
| Valence states C | $2s, 2p$ |
| Valence states Si | $3s, 3p$ |
| **k**-point mesh | $2 \times 2 \times 2$ |
| Lattice parameters | $a = b = c = 4.39$ Å |
| Band-gap energy | 1.35 eV |
| Madelung constant | 1.638 |
| $\epsilon_0$ | 9.72 [56] |

TABLE II. Parameters used in the calculations of the positron lifetimes in the two considered polytypes. For the high-frequency dielectric constant of $6H$-SiC, we use the average of the experimental values in ordinary and extraordinary directions.

| Positron lifetimes | |
| --- | --- |
| Polytype | $3C$-SiC |
| e-e x-c functional | LDA |
| Atomic sites | 216 |
| $E_{cut}$ | 600 eV |
| Valence states C | $2s, 2p$ |
| Valence states Si | $2s, 2p, 3s, 3p$ |
| **k**-point mesh | $2 \times 2 \times 2$ |
| Lattice parameters | $a = b = c = 4.33$ Å |
| $\epsilon_\infty$ | 6.52 [56] |
| Polytype | $6H$-SiC |
| e-e x-c functional | LDA |
| Atomic sites | 192 |
| $E_{cut}$ | 600 eV |
| Valence states C | $2s, 2p$ |
| Valence states Si | $2s, 2p, 3s, 3p$ |
| **k**-point mesh | $4 \times 4 \times 2$ |
| Lattice parameters | $a = b = 3.06$ Å |
| | $c = 15.03$ Å |
| $\epsilon_\infty$ | 6.61 [56] |

216-, and 512-atom cells. We obtained 288, 270, and 270 ps, respectively. With the difference between the results obtained in 216- and 512-atom supercells being smaller than 1 ps, we conclude that the $3 \times 3 \times 3$ cell is large enough for the positron lifetime calculations.

### IV. EPR EXPERIMENTS RESULTS

For all annealing temperatures, EPR measurements were performed at both 80 and 300 K. Here, we only present the results obtained at 300 K since the measured concentrations were similar in the two cases for all annealing temperatures.

### A. EPR on as-irradiated crystals

Before annealing, measurements at 300 K show the presence of three main paramagnetic centers (see Fig. 1). The first one (inset of Fig. 1) is isotropic with a $g_{iso} = 2.0032$ central line surrounded by two sets of HF lines, which intensities correspond to the interaction with 12 equivalent silicon neighbors. This is characteristic of a defect located into a silicon site, which has 12 Si atoms as second neighbors. This signal does not exhibit any zero-field splitting (ZFS). It has already been detected after irradiation with various particles [19,57,58] and attributed to the isolated $V_{Si}^{1-}$ with a spin $S = \frac{3}{2}$. This signal is in fact a superposition of signals coming from hexagonal and quasicubic sites which can not be distinguished using an $X$-band spectrometer. This signal is called $V_{Si}^{1-}$ in the following. The $V_{Si}^{1-}$ concentration in the as-irradiated crystals is $2.2(\pm 0.3) \times 10^{17}$ cm$^{-3}$.

The two other detected signals are composed of a doublet with a ZFS of approximately 20 and 90 G for $B \parallel c$. Their $g$ factor is isotropic and equal to 2.0032. They have also been detected after irradiation in various conditions [19,57,58] and have been named $K_{y2}$. They were first attributed [59] to the neutral $V_{Si}^0$ with a spin $S = 1$, in one hexagonal site for $D = 90$ G and two quasicubic sites for $D = 20$ G (the signals relative to the two quasicubic sites can not be separated using an $X$-band spectrometer). A recent study by Mizuochi *et al.* [60] concerning the $T_{V2a}$ signal (equivalent to the $K_{y2}$ signal for the $4H$ polytype), however, contradicts this assignment as they clearly showed that the spin state of the defect is $S = \frac{3}{2}$. Consequently, this defect is now proposed to be another, more distorted, state of the negatively charged silicon vacancy, which could explain the differences concerning the Hamiltonian parameters compared with the $V_{Si}^{1-}$ signal, particularly the ZFS. This distortion may be due to the presence of an impurity or of another defect located at some distance along the $c$ axis ([0001]) [57]. The signal is called $V_{Si}^{1-}$dis (as "distorted") in the following. The $V_{Si}^{1-}$dis concentration in the as-irradiated crystals is $2.6(\pm 0.3) \times 10^{17}$ cm$^{-3}$.

### B. EPR on annealed samples

For all annealing temperatures, the EPR measurements performed at 300 K show the presence of the three paramagnetic centers described in the previous section and related to the silicon vacancy. Figure 2 shows the evolution of the concentrations of $V_{Si}^{1-}$ and $V_{Si}^{1-}$dis as a function of the annealing temperature.

The distorted silicon vacancy $V_{Si}^{1-}$dis concentration decreases from around $2.4 \times 10^{17}$ cm$^{-3}$ down to $1.6(\pm 0.3) \times 10^{16}$ cm$^{-3}$ during annealing. The silicon vacancy $V_{Si}^{1-}$ concentration is first stable at $2.2(\pm 0.3) \times 10^{17}$ cm$^{-3}$, then decreases first to $1.4 \times 10^{17}$ cm$^{-3}$ and later to $6.7(\pm 1.0) \times 10^{15}$ cm$^{-3}$. The total silicon vacancy concentration [$V_{Si}^{1-}$tot] is first nearly constant around $4.5(\pm 0.6) \times 10^{17}$ cm$^{-3}$ and then decreases down to $1.2(\pm 0.1) \times 10^{16}$ cm$^{-3}$. We can observe that all three concentrations become relatively low above approximately 600 °C, which means that the silicon vacancies recombine or cluster in the sample.

### V. PAS RESULTS

For all annealing temperatures, the average lifetime in the sample is longer than the SiC lattice value. Two lifetime components are extracted from the lifetime spectra recorded at each measurement temperature. The decompositions have first been performed using two free lifetime components ($\tau_1$ and $\tau_2$). The short component $\tau_1$ remained then almost constant at the $140 \pm 10$ ps value for the whole range of the measurement temperatures. For a better accuracy on the other parameters, the decompositions reported in this paper have therefore been performed with $\tau_1$ fixed at the 140-ps value. It has been checked that neither the average lifetime nor the variance of the decomposition is affected by this choice. This method will, however, reduce artificially the error bars on the determination of the long-lifetime component and of its intensity from the ranges $\pm 5$ ps or $\pm 5\%$ to $\pm 1$ ps or $\pm 1\%$.

### A. Evidence for the detection of negatively charged nonvacancy defects

For all annealing and measurement temperatures, two components are obtained from the decomposition. The short-lifetime component $\tau_1$ is close to the $6H$-SiC lattice lifetime ($\tau_L = 140$ ps [17]). This lifetime indicates the detection of negatively charged nonvacancy defects (also called "negative ions"), as the electronic density around negative ions is close to the density observed around the atoms in the lattice [35]. As described in the paper related to the as-irradiated samples [17], two types of negative ions are in fact detected in the crystals. One of them was already detected in the as-grown crystals, and the other one was generated by irradiation.

Moreover, the second lifetime component $\tau_2$ is much longer than the lattice lifetime for all measurement and annealing temperatures. This indicates trapping in vacancy defects. In that case, if some of the positrons had annihilated in a nonlocalized state (i.e., in the lattice), the short-lifetime component $\tau_1$ values would have been shorter than the lattice lifetime (the mean time spent in the lattice is shorter due to the trapping inside the defects). Then, the values of $\tau_1$ indicate a total trapping of the positrons in defects, both into vacancy defects and "negative ions," even after 1050 °C annealing.

### B. Lifetime components as a function of the measurement temperature

The evolution of the lifetime components as a function of the measurement temperature for various annealing temperatures is plotted in Fig. 3. For each annealing temperature, the values of the average positron lifetime $\tau_{av}$ [Fig. 3(a)], the long-lifetime component $\tau_2$ [Fig. 3(b)], and its relative intensity $I_2$ [Fig. 3(c)] are plotted as a function of measurement temperature. The presented parameters are relative to the measurements performed before and after annealing at 300 °C, 750 °C, 850 °C, and 1000 °C. These annealing temperatures were chosen because the evolution of the positron lifetime parameters as a function of the measurement temperature is representative of the general behavior.

In the as-irradiated crystals, no strong variation is observed in the positron characteristics when the measurement temperature changes. The average lifetime increases slightly from $202 \pm 1$ ps to $205 \pm 1$ ps between 15 and 295 K. The long-lifetime component $\tau_2$ rises from $214 \pm 2$ to $218 \pm 2$ ps in the measurement temperature range and its intensity is stable at $83 \pm 2\%$.

It must be stressed that the as-irradiated samples have already been characterized by Henry *et al.* [17]. In that study, however, a different spectrometer and source were used. The lifetime spectra decompositions were, therefore, slightly different. In Ref. [17], $\tau_{av}$ was increasing from $204 \pm 1$ to $207 \pm 1$ ps and $\tau_2$ from $225 \pm 2$ to $229 \pm 2$ ps. The average lifetime is, at the maximum, 2 ps lower in the new experiment series and is combined with a lower value of the long-lifetime component $\tau_2$. The same main conclusions can be drawn from the two experiments series, i.e., more than one vacancy defect is detected in the as-irradiated samples, one of which being preponderant.

After annealing at 300 °C, $\tau_{av}$ first increases slightly from $194 \pm 1$ ps up to $198 \pm 1$ ps and then reaches $208 \pm 1$ ps at

6H-SiC CREE n-type ($n_D$-$n_A$=1,9x10$^{-17}$ cm$^{-3}$)
proton irradiated (E=12 MeV, fluence=4x10$^{16}$ cm$^{-2}$)
▼  as-irradiated
▲  300°C annealed
■  750°C annealed
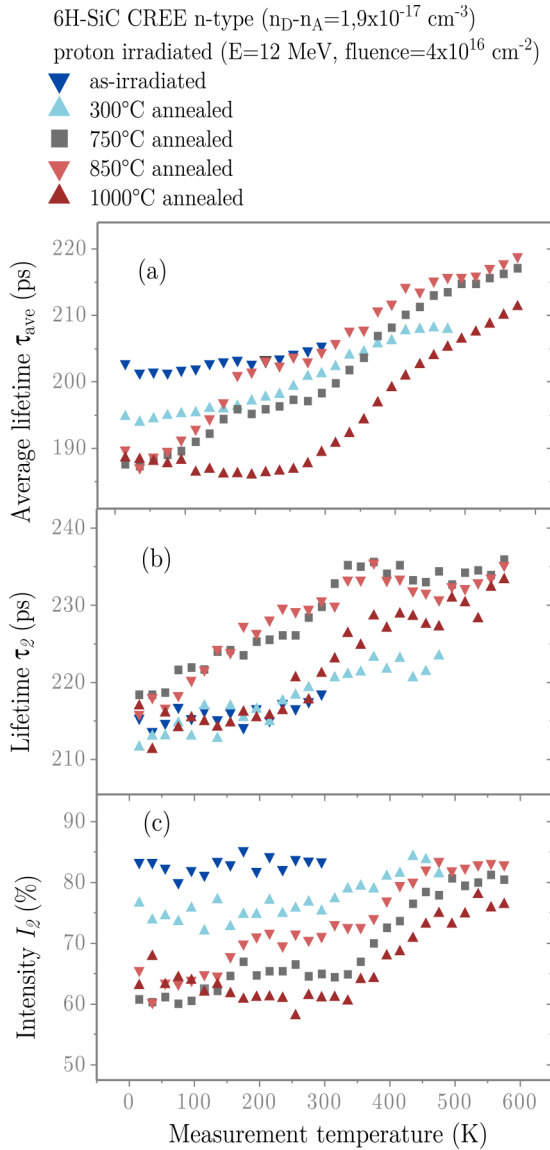▼  850°C annealed
▲  1000°C annealed



FIG. 3. (Color online) Measurement temperature dependence of the positron lifetime components obtained for the 12-MeV proton as-irradiated crystals, and after different annealing steps: (a) average lifetime $\tau_{av}$; (b) lifetime $\tau_2$ of the longest component; (c) its intensity $I_2$. The uncertainty on the values is close to the symbol size.

various defects is induced by a variation in their concentration, or by a change in the nature of the detected defects, but not by a modification of their charge states. $\tau_2$ measured in the 300 °C annealed crystals varies from 212 to 222 ps when the measurement temperature changes from 15 to 475 K. These values are close to the lifetimes measured in the as-irradiated crystals and the population of defects should be very similar to at in as-irradiated samples. However, the $I_2$ intensity is lower after annealing at 300 °C. It suggests that the concentration of vacancy-type defects has decreased during annealing.

After annealing at 750 °C, the average positron lifetime first increases from $188 \pm 1$ to $196 \pm 1$ ps and is then stable between 175 and 275 K. It then rises again and reaches $217 \pm 1$ ps value at 575 K. $\tau_2$ increases from $218 \pm 2$ to $235 \pm 3$ ps when the temperature increases. We can also observe an increase of the intensity $I_2$ around 350 K. A rather similar evolution of the three characteristics $\tau_{av}$, $\tau_2$, and $I_2$ is also observed after annealing at 850 °C.

The average lifetime $\tau_{av}$ measured in the 750 °C annealed crystals increases very strongly, from 188 to 217 ps, in the 15–575 K measurement temperature range. It indicates a modification of the distribution of the vacancy defects detected in the samples. In addition, $\tau_2$ increases from 218 to 235 ps when the measurement temperature increases from 15 to 475 K. These values are very different from the lifetimes measured before and after annealing at 300 °C. At higher temperatures, $\tau_2$ values form a plateau at 235 ps. This lifetime is also observed at different annealing temperatures. These two points suggest that the 235-ps lifetime is characteristic of a vacancy defect, which we will call $V_A$. The change of $\tau_2$ with temperature indicates that at least one of the vacancy defects detected at low temperature is negatively charged, while the $V_A$ defect detected at high temperatures is neutral. The negatively charged vacancy will be called $V_B$ in the following.

After annealing at 750 °C, $I_2$ is close to 60% in the 15–335 K measurement temperature range, while it is equal to 75% after annealing at 300 °C. For higher measurement temperatures, $I_2$ values remain close to 80%. It indicates that the trapping rate at vacancy defects decreased at low measurement temperature, while it remained constant at high temperature. Two phenomena could explain the decrease of the trapping rate at vacancy defects in the low-temperature range: an increase of the "negative ions" concentration or a decrease of the $V_B$ concentration. EPR measurements indicate that the isolated negative silicon monovacancy concentration has strongly decreased for annealings performed between 300 °C and 750 °C and is very small after annealing at 750 °C. The $I_2$ decrease therefore probably results from the $[V_{Si}^{1-}]$ decrease. We propose, hence, that the negatively charged vacancy defect $V_B$ is the silicon monovacancy.

After annealing at 850 °C, $\tau_{av}$ first increases from $188 \pm 1$ ps up to $202 \pm 1$ ps between 15 and 175 K. It is then stable until 275 K and increases again until 575 K reaching $219 \pm 1$ ps. $\tau_2$ increases from $216 \pm 2$ to $233 \pm 3$ ps between 15 and 375 K and it remains stable until 575 K. Its relative intensity $I_2$ is first stable at $64 \pm 2\%$ between 15 and 135 K, then it increases until 215 K and $72 \pm 2\%$. It is stable until 355 K, then increases again until $82 \pm 2\%$ at 475 K and it finally remains stable until 575 K.

415 K and remains stable. $\tau_2$ increases from $212 \pm 2$ ps up to $222 \pm 2$ ps, while its intensity changes from $75 \pm 3\%$ to $83 \pm 2\%$.

The average lifetime $\tau_{av}$ measured in the crystals annealed at 300 °C varies more strongly (from 194 to 208 ps) than in the as-irradiated crystals as a function of the measurement temperature. It indicates a modification of the distribution of the vacancy defects and/or of the "negative ions" detected in the crystals. The long-lifetime component $\tau_2$ values are characteristic of the distribution of the vacancy defects detected in the crystals. For a given annealing temperature, EPR measurements show that the isolated silicon vacancy concentration remains constant for all measurement temperatures, which indicates that the Fermi level does not vary. We propose, therefore, that the modification of the trapping rate of the

The values of the average lifetime $\tau_{av}$, of the long-lifetime component $\tau_2$, and of its relative intensity $I_2$ measured in the samples annealed at 850 °C are very close to the ones measured after annealing at 750 °C, except in the 175–335 K measurement temperature range. In this range, $\tau_{av}$ is 6 ps higher than the ones measured after annealing at 750 °C. While the $\tau_2$ lifetimes are almost identical, $I_2$ values are higher than the ones measured after annealing at 750 °C. This indicates that the trapping rate in vacancy defects increases relatively to the trapping rate around the "negative ions." The $I_2$ increase can result from a change in the trapping rates coefficients or in the concentration of the negative ions or of the vacancy defects. The values of $\tau_2$ are almost identical, even at low measurement temperature, where the trapping in the neutral defect called $V_A$ is in competition with the trapping in $V_{Si}^{1-}$. It suggests that the nature (and therefore the trapping coefficient) and the concentration of the vacancy defects changed only slightly between annealing at 750 °C and 850 °C. Meanwhile, the silicon vacancies concentrations measured using EPR after annealing at 750 °C and 850°C are close (respectively $8 \times 10^{16}$ cm$^{-3}$ and $6 \times 10^{16}$ cm$^{-3}$). $I_2$ variations therefore result from a decrease in the negative ion concentration between 750 °C and 850 °C, while the vacancy defects distribution remains almost identical.

Finally, after annealing at 1000 °C, $\tau_{av}$ is first stable at $188 \pm 2$ ps and then starts rising at around 300 K to finally reach $211 \pm 1$ ps. The long-lifetime component $\tau_2$ varies between $216 \pm 2$ and $231 \pm 3$ ps. The intensity corresponding to this lifetime is first stable and then starts rising at around 350 K to reach $76 \pm 2\%$ at 575 K.

The average lifetime $\tau_{av}$ in the 1000 °C annealed crystals is 6 to 15 ps shorter than after 850 °C annealing. This suggests a change in the distribution of the vacancy defects detected in the samples. The $\tau_2$ lifetime measured in these crystals is first stable around 215 ps for measurement temperatures lower than 235 K and then increases until 575 K reaching 231 ps. These values differ from the ones measured after annealing at 850 °C. The 215-ps lifetime, measured at low temperature, corresponds probably to the positron trapping in negative silicon vacancies. At higher measurement temperatures, the values of $\tau_2$ are around 231 ps, which is slightly shorter than the $V_A$ characteristic lifetime is detected for lower annealing temperatures.

### C. Lifetime components as a function of the annealing temperature

For all annealing temperatures, $\tau_{av}$ and $\tau_2$ vary with the measurement temperature. This indicates that at least one negative defect is detected. Moreover, since the long-lifetime component depends on the annealing temperature, we assume that several types of vacancy defects are detected and their concentrations change during annealing. We choose to present the evolutions of the spectra as a function of annealing temperature for three characteristic measurement temperatures: 35, 215, and 555 K (see Fig. 4). The low (35 K) and high (575 K) measurement temperatures enable us to obtain information on the negatively charged and the neutral vacancy defects detected in the crystals, respectively. For a better accuracy, the values presented for 35 K are in fact an average for 15, 35, and 55 K,
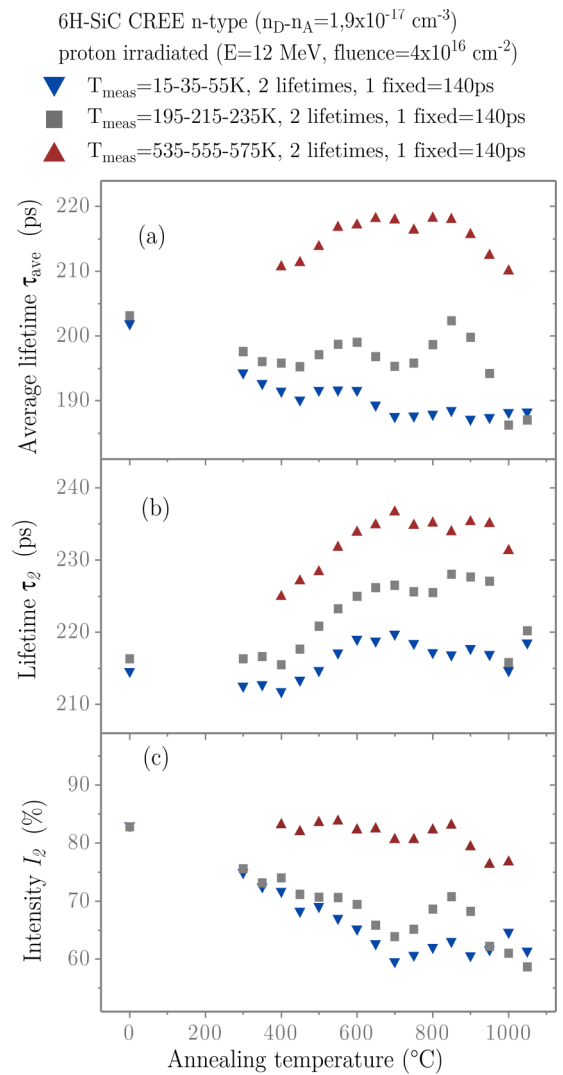


FIG. 4. (Color online) Annealing temperature dependence of the positron lifetime components obtained for the 12-MeV proton irradiated crystals for three different measurement temperatures: (a) average lifetime $\tau_{av}$; (b) lifetime $\tau_2$ of the longest component; (c) its intensity $I_2$.

the values for 215 K are an average for 195, 215, and 235 K and the values for 555 K are an average for 535, 555, and 575 K.

For low measurement temperatures, the average lifetime decreases from $202 \pm 1$ to $188 \pm 1$ ps as a function of annealing temperature. $\tau_2$ is first stable at around $213 \pm 2$ ps up to 450 °C, then increases up to 700 °C where it reaches $219 \pm 2$ ps and then starts decreasing. The intensity corresponding to this lifetime component decreases up to 700 °C and then remains stable at $60 \pm 2\%$.

For measurements performed at 215 K, the evolution of the average lifetime is more complex. The lifetime first decreases from $203 \pm 1$ to $195 \pm 1$ ps, then rises up to $199 \pm 1$ ps and decreases again down to $195 \pm 1$ ps. When the annealing temperature increases, it rises again to reach $202 \pm 1$ ps and then it decreases abruptly to $186 \pm 1$ ps. The long-lifetime component is first stable at around $216 \pm 2$ ps, then rises between 400 °C and 700 °C and becomes stable again at around $226 \pm 3$ ps up to 950 °C.

At high measurement temperatures, $\tau_{av}$ first increases from $211 \pm 1$ ps up to $218 \pm 1$ ps, then is stable between 700 °C and 850 °C and finally decreases to $210 \pm 1$ ps. $\tau_2$ first increases from $225 \pm 2$ ps up to $235 \pm 3$ ps between 400 °C and 700 °C and then remains stable at around $231 \pm 2$ ps. Its relative intensity $I_2$ is high and remains stable at $82 \pm 2\%$ between 400 °C and 850 °C and then decreases slightly to $76 \pm 2\%$.

## VI. CALCULATIONS RESULTS

### A. Charge state calculations

We calculated the formation energies of several vacancy complexes in 3*C*-SiC with charges varying from $-2$ to $+2$. Calculations were performed for six different defects: $V_C + V_C$, $V_C + V_{Si}$, $V_{Si} + V_C + C_{Si}$, $V_C + V_{Si} + V_C$, $V_{Si} + V_C + V_{Si}$, and $(V_C + V_{Si})_2$. We initially considered a silicon divacancy $V_{Si} + V_{Si}$, but with the positron localized inside, this defect transformed into a $V_{Si} + V_C + C_{Si}$ complex, hence, this latter defect was studied instead.

The variation of the formation energies as a function of the electron chemical potential are presented in Figs. 5(a)–5(f). All results are extrapolated to the theoretical gap edge of 6*H*-SiC (2.01 eV), as it has been shown that the results in the hexagonal polytype can be obtained from those in the 3*C*-SiC using this kind of extrapolation [28]. We can observe that the carbon divacancy $V_C + V_C$ has a positive charge in a wide range of Fermi levels. It should thus be difficult to observe this defect in 3*C*-SiC and in the hexagonal polytype it could be only detected in *n*-type samples. The $V_C + V_{Si}$ divacancy is found to be neutral for a wide range of $\mu_e$. It is consistent with the fact that this is a stoichiometric defect. This defect should

be mostly neutral if detected in 3*C*-SiC, while in 6*H*-SiC it should be neutral for undoped or slightly doped samples and negative in more *n*-doped samples. The $V_{Si} + V_C + C_{Si}$ complex has a positive charge state only for Fermi levels laying close to the maximum of the valence band and should therefore be possible to detect in undoped and *n*-type samples in both polytypes. The $V_C + V_{Si} + V_C$ trivacancy should be possible to detect in *n*-type 3*C*-SiC and in undoped and *n*-doped 6*H*-SiC. The second trivacancy $V_{Si} + V_C + V_{Si}$ is negative for the majority of possible Fermi levels and should, hence, strongly attract the positrons if present in the material. Finally, the $(V_C + V_{Si})_2$ tetravacancy, which is also a stoichiometric defect, has a narrower range of the neutral charge stability. This defect, however, should be neutral in undoped 3*C*-SiC. In 6*H*-SiC it can start to have a $-1$ charge state for Fermi levels close to the middle of the band gap.

To enable the comparison between the studied defects, we present in Fig. 6 the formation energies of the most stable charge states of all defects. Additionally, we recall in this figure the results obtained for the monovacancies in Ref. [28]. These results were obtained in the 3*C* polytype and are extrapolated to the theoretical gap edge of 6*H*-SiC (2.01 eV).

Several theoretical studies [6,61,62] showed that the silicon vacancy in silicon carbide is a high-spin defect. Similarly, high-spin states are also expected for the vacancy clusters containing $V_{Si}$. In Table III, we present the calculated spin states of the vacancy clusters in 3*C*-SiC, which can be useful for the EPR measurements interpretations. The results presented in Table III show that the majority of the considered defects (types and their charge states) should have a nonzero spin and it should be possible to detect them in EPR. It is
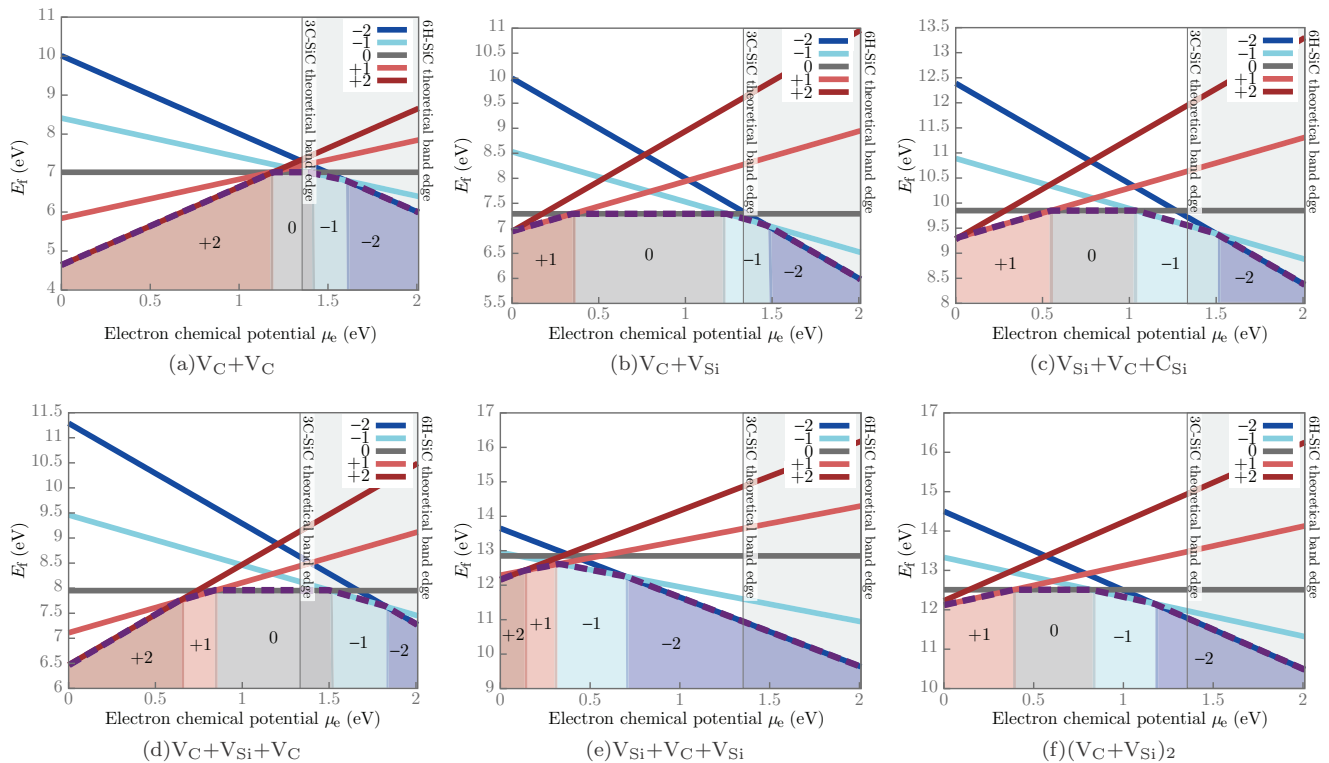


FIG. 5. (Color online) Formation energies of various charge states of vacancy complexes calculated in stoichiometric 3*C*-SiC (white background). Results are extrapolated to the top of the 6*H*-SiC gap (gray background).
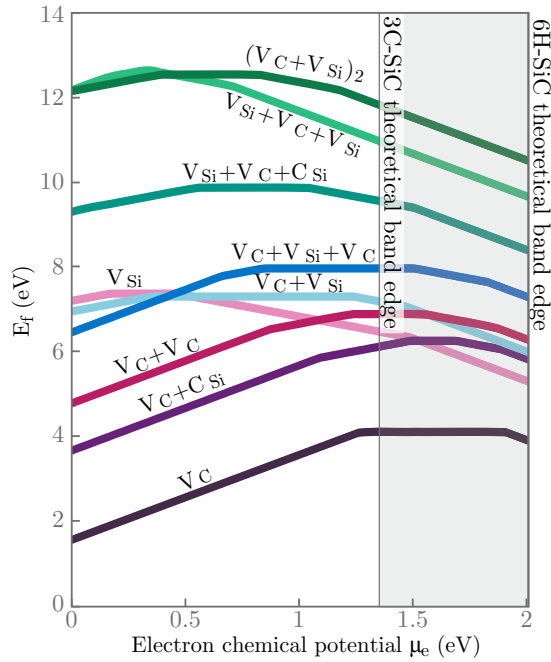
FIG. 6. (Color online) Formation energies of the most stable charge states of the vacancy complexes studied in stoichiometric $3C$-SiC (white background). Results are extrapolated to the top of the $6H$-SiC gap (gray background).

consistent with the fact that several types of defects were detected in SiC using this method [19–26]. In our study, however, we did not detect any EPR signal corresponding to the defect clusters.

### B. Positron lifetimes calculations

#### 1. 3C-SiC

We calculated the positron lifetimes of all neutral vacancy complexes in $3C$-SiC containing from two to six vacancies. As the lattice lifetime obtained in our calculations is slightly longer than the experimental one (144 ps compared to 140 ps [17]), we also present the lifetimes scaled to this experimental value. The results are presented in Table IV and compared with the results obtained previously by Brauer *et al.* [5,13]. In these latter calculations, the superimposed atom model was used and the atomic relaxation and the influence of the positron on the electronic density were not taken into account.

TABLE III. Calculated spin states of defect clusters in $3C$-SiC.

| Defect | Charge state | | | | |
| --- | --- | --- | --- | --- | --- |
| | $-2$ | $-1$ | $0$ | $+1$ | $+2$ |
| $V_C + V_C$ | 0 | 1/2 | 0 | 1/2 | 0 |
| $V_C + V_{Si}$ | 0 | 1/2 | 1 | 1/2 | 0 |
| $V_{Si} + V_C + C_{Si}$ | 1 | 1/2 | 1 | 1/2 | 0 |
| $V_C + V_{Si} + V_C$ | 1 | 1/2 | 2 | 1/2 | 1 |
| $V_{Si} + V_C + V_{Si}$ | 2 | 5/2 | 3 | 5/2 | 0 |
| $(V_C + V_{Si})_2$ | 1 | 3/2 | 2 | 3/2 | 1 |

TABLE IV. Positron lifetimes of the relaxed neutral defect clusters in $3C$-SiC. The results are presented along with the lattice and monovacancies lifetimes from Ref. [28] and compared with results of Brauer *et al.* [5,13]. Additionally to the calculated values we present the lifetimes scaled to the experimental lattice lifetime of 140 ps [17].

| Defect | Lifetime PSN (ps) | Scaled lifetime (ps) | Lifetime Refs. [5,13] |
| --- | --- | --- | --- |
| Lattice | 144 | 140 | 141 |
| $V_C$ | 195 | 190 | 150 |
| $V_{Si}$ | 227 | 221 | 185 |
| $V_C + C_{Si}$ | 203 | 197 | |
| $V_C + V_C$ | 201 | 195 | |
| $V_C + V_{Si}$ | 242 | 235 | 216 |
| $V_{Si} + V_C + C_{Si}$ | 245 | 238 | |
| $V_C + V_{Si} + V_C$ | 250 | 243 | |
| $V_{Si} + V_C + V_{Si}$ | 269 | 262 | |
| $(V_C + V_{Si})_2$ | 269 | 262 | 254 |
| $(V_C + V_{Si})_3^{chain}$ | 270 | 263 | 286[a] |
| $(V_C + V_{Si})_3^{ring}$ | 304 | 296 | 286[a] |

[a]In the reference, the configuration of the cluster is not specified.

As was shown before [28], the relaxation effect is important in calculations for SiC. We find longer lifetimes than in the study of Brauer *et al.* because all defects relaxed outwards in our study. We can observe that the differences between the two sets of calculations decrease when the cluster size increases. The fact that the relaxation decreases for larger defects is consistent with what was shown, for example, for vacancy clusters in Si [29,63,64].

It can be noticed that in some cases, the positron lifetimes can be very similar for different defects. For $V_C$, $V_C + C_{Si}$, and $V_C + V_C$ we find lifetimes of 195, 203, and 201 ps, respectively. This can be explained by the fact that, in all of these defects, the positron density is localized at one carbon atomic site, as shown in Fig. 7. Additionally, it is worth noting that in the $V_C + V_C$ divacancy, the positron is localized in one of the two defects. It means that this cluster, in which the two vacancies are second neighbors, is seen as two separated defects by the positron.

Similarly, lifetimes of 242, 245, and 250 ps were found for the $V_C + V_{Si}$, $V_{Si} + V_C + C_{Si}$, and $V_C + V_{Si} + V_C$ clusters, respectively. All these defects contain one silicon vacancy and the positron density is localized at its site (see Fig. 8).
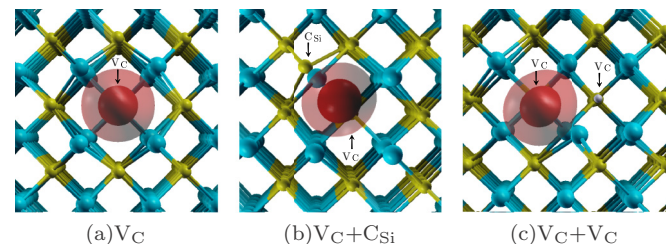


(a) $V_C$ (b) $V_C + C_{Si}$ (c) $V_C + V_C$

FIG. 7. (Color online) Positron isodensities (solid traced for 70% of the maximum density, transparent for 30%), in red, in $V_C$, $V_C + C_{Si}$, and $V_C + V_C$, in $3C$-SiC. Figures were generated using XCRYSDEN [66,67] program.

(a)$V_{Si}$

(b)$V_C$+$V_{Si}$

(c)$V_{Si}$+$V_C$+$C_{Si}$
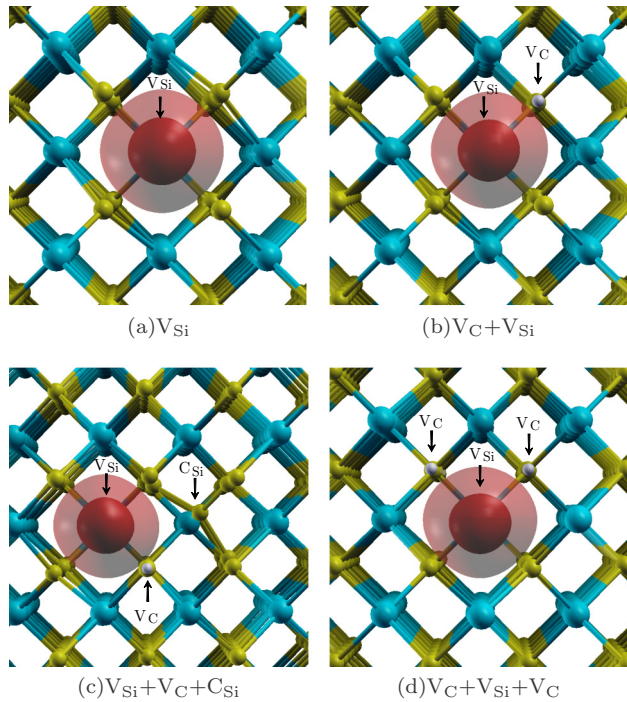
(d)$V_C$+$V_{Si}$+$V_C$

FIG. 8. (Color online) Positron isodensities (solid traced for 70% of the maximum density, transparent for 30%), in red, in the defects containing one silicon vacancy, in 3*C*-SiC. Carbon atoms are presented in yellow, silicon atoms in blue. White spheres represent the carbon vacancies. Figures were generated using XCRYSDEN [66,67] program.

Additionally, the density has a similar spherical form in all of these defects and it is almost not affected by the presence of carbon vacancies nor by a carbon atom in the antisite position, in the case of $V_{Si}$ + $V_C$ + $C_{Si}$.

For the two defects containing two silicon vacancies, $V_{Si}$ + $V_C$ + $V_{Si}$ and $(V_C + V_{Si})_2$, the same lifetime of 269 ps was found. As in the case of defects with one $V_{Si}$ only, the positron density is not sensitive to the additional carbon vacancy (Fig. 9) and is situated between the two silicon vacancies. It is worth



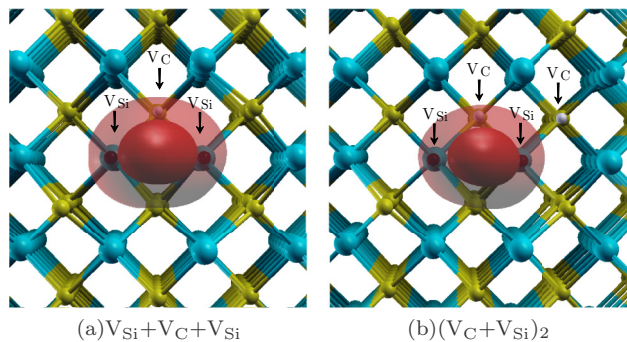(a)$V_{Si}$+$V_C$+$V_{Si}$

(b)$(V_C$+$V_{Si})_2$

FIG. 9. (Color online) Positron isodensities (solid traced for 70% of the maximum density, transparent for 30%), in red, in the defects containing two silicon vacancies, in 3*C*-SiC. Carbon atoms are presented in yellow, silicon atoms in blue. Carbon and silicon vacancies are represented by white and black spheres, respectively. Figures were generated using XCRYSDEN [66,67] program.



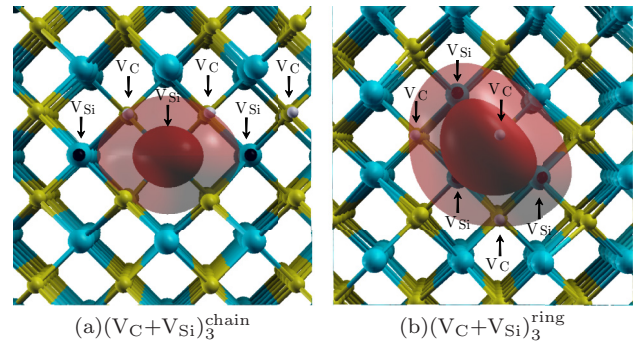(a)$(V_C$+$V_{Si})_3^{chain}$

(b)$(V_C$+$V_{Si})_3^{ring}$

FIG. 10. (Color online) Positron isodensities (solid traced for 70% of the maximum density, transparent for 30%), in red, in two configurations of a hexavacancy, in 3*C*-SiC. Carbon atoms are presented in yellow, silicon atoms in blue. Carbon and silicon vacancies are represented by white and black spheres, respectively. Figures were generated using XCRYSDEN [66,67] program.

noting that for the $(V_C + V_{Si})_2$ defect various configurations are possible, with different distances between the furthest Si and C vacancies. However, for all these configurations, the $V_{Si}$-$V_{Si}$ distance is the same and since the positron is not sensitive to the position of the additional carbon vacancy, lifetimes of these configurations were found to differ by less than 1 ps.

For the $(V_C + V_{Si})_3$ defect, even more different configurations are possible than for $(V_C + V_{Si})_2$. Additionally, in these configurations, the silicon vacancies are not distributed in the same way. We studied the two extreme cases, a chain and a ring configuration (see Fig. 10). We found the lifetimes of 270 ps for the first one and 304 ps for the second one. In the chain $(V_C + V_{Si})_3$, the three silicon vacancies form a line and the positron is localized in the central silicon vacancy [see Fig. 10(a)]. In the ring hexavacancy, the three silicon vacancies form a triangle inside which the positron is localized [see Fig. 10(b)]. We can observe that the positron lifetimes calculated for these two configurations of the hexavacancy differ strongly. Moreover, the lifetime calculated for the ring hexavacancy is close to the one calculated for the tetravacancy (269 ps).

To determine which configuration of the hexavacancy is more stable, we calculated their formation energies. We found 15.16 and 17.79 eV for the neutral charge states of the ring and chain configurations, respectively. It suggests that the ring structure is more stable and will more likely be formed in the material. It has to be kept in mind, however, that the calculations were performed for the neutral charge state only and that the relative stability of these configurations may depend on the charge state and the position of the Fermi level.

### 2. 6*H*-SiC

In our previous study on smaller defects in SiC [28] we observed that in the case of the carbon vacancy, the positron lifetime differs between the polytypes and between the three possible sites in 6*H*-SiC. For the silicon vacancy, these differences were around 1 ps. To verify whether the positron lifetimes of the vacancy complexes depend on the polytype or on the atomic sites in the case of 6*H*-SiC, we performed calculations for all possible configurations of the $V_C + V_{Si}$ divacancy in the hexagonal polytype. Results are presented in

TABLE V. Comparison of positron lifetimes of divacancies in $3C$-SiC and $6H$-SiC. Lifetimes scaled to the experimental lattice lifetime of 140 ps [17] are presented in parentheses.

| | Site | Lifetime PSN (ps) |
|---|---|---|
| Lattice | $3C$ | 144 |
| $V_C + V_{Si}$ | $3C$ | 242 (235) |
| Lattice | 6H | 143 |
| $V_C + V_{Si}$ | $6H_{h-h}$ | 241 (236) |
| $V_C + V_{Si}$ | $6H_{k_1-k_1}$ | 240 (235) |
| $V_C + V_{Si}$ | $6H_{k_2-k_2}$ | 239 (234) |
| $V_C + V_{Si}$ | $6H_{k_1-k_2}$ | 240 (235) |
| $V_C + V_{Si}$ | $6H_{h-k_1}$ | 241 (236) |
| $V_C + V_{Si}$ | $6H_{k_2-h}$ | 241 (236) |

Table V. We observe that all lifetimes of divacancies in $6H$-SiC are very similar, with differences between 1 and 2 ps, and close to the lifetime of this defect in $3C$-SiC. These results suggest that the positron lifetimes calculated for vacancy complexes in $3C$-SiC can be used for the interpretation of the PAS experiments performed on the $6H$-SiC samples as well.

## VII. DISCUSSION

The EPR measurements indicate the presence of $V_{Si}^{1-}$ in the studied samples. This defect was especially observed in the as-irradiated samples and for low annealing temperatures. Meanwhile, the PAS measurements for the as-irradiated samples showed a lifetime of $214 \pm 2$ to $218 \pm 2$ ps. This lifetime is very close to the 219-ps lifetime recently calculated for the $V_{Si}^{1-}$ in $6H$-SiC [65] (when scaled to the experimental lattice lifetime). The results of both the EPR and PAS measurements thus indicate that the silicon vacancy is probably the main defect observed by these methods before annealing and at low temperatures after annealing.

The PAS measurements at 215 K (see Fig. 4) show that the positron lifetime is stable for annealing temperatures lower than 400 °C, then starts increasing and stabilizes around 650 °C. For similar temperatures, the EPR signal (see Fig. 2) attributed to the silicon vacancy decreases. This indicates that at these temperatures, the silicon vacancy is annealed and that a larger defect exhibiting a longer lifetime is created. This defect is probably neutral because it is observed at high measurement temperatures, when the trapping coefficient depends more on the size of the defect than on its charge. Additionally, it has to contain at least part of the disappearing silicon vacancies.

At high measurement temperatures, the negative defect should not be predominant in the PAS signal any longer and the neutral cluster (that we previously called $V_A$) should be mostly detected, due to its larger volume. In Fig. 4, we can notice that $\tau_2$ increases between the annealing temperatures of 400 °C and 700 °C for 555-K measurements. We propose that during this stage the silicon vacancy is annealed through clustering. The long-lifetime component stabilizes at 235 ps. This lifetime is very close to the one we calculated for the neutral $V_C + V_{Si}$ divacancy (235 ps in $3C$-SiC and between 234 and 236 ps in $6H$-SiC, when scaled to the experimental lattice lifetime). Additionally, our charge state calculations

showed that the divacancy should be neutral in a wide range of electron chemical potentials [see Fig. 5(b)].

Therefore, we propose that the $V_A$ defect is the neutral $V_C + V_{Si}$ divacancy. This suggests that in the studied $6H$-SiC samples, silicon vacancies were created by irradiation and were then annealed between 400 °C and 700 °C. The annealing was probably due to formation of $V_C + V_{Si}$. This process requires migration of carbon or silicon vacancies. According to Zolnai *et al.* [68], the carbon monovacancies migration is only possible for annealing temperatures higher than 1100 °C. Additionally, *ab initio* calculations of Bockstedte *et al.* [9] yielded a significantly higher migration barrier for the $V_C^{2+}$ vacancy (5.2 eV) than for $V_{Si}^{1-}$ (3.2 eV). Therefore, we propose that the process was related to silicon vacancies migration. This should, however, be confirmed by additional experimental and theoretical studies. We also assume that the carbon vacancies, that are indispensable in the clusters formation, were also created by irradiation, but that they could not be detected by the characterization methods used. Their most probable charge states, 0 and 2+ [28], are nonparamagnetic and can not be observed in EPR. As for the PAS, the positive carbon vacancies do not trap positrons and the neutral ones would trap much less positrons than the negative silicon vacancies, inducing a very weak signal.

Our results can be compared with the EPR study of Carlsson *et al.* [26]. They observed a strong annealing of silicon vacancies in irradiated $4H$-SiC up to 700 °C and simultaneous increase in the $V_C + V_{Si}$ divacancy concentration. This behavior is in good agreement with what we observe in irradiated $6H$-SiC samples. It is worth noting that in our study, the divacancies were detected by PAS and not EPR. We suppose that the intensity of the $P6/P7$ center ($V_C + V_{Si}$ divacancy) was too weak to identify it in the as-received samples and has not been tracked in the annealed crystals.

As for the behavior of the "negative ions," we observe that the long-lifetime component $\tau_2$ measured at 215 K remains constant during annealing at temperatures between 700 °C and 850 °C. Meanwhile, its relative intensity $I_2$ increases. It indicates that in this annealing temperature range, the trapping rate in the vacancy defects increases. The increase of the $I_2$ values measured at 555 K is much smaller because at this measurement temperature, the positron trapping around negative ions is not dominant. We propose that this process is the annealing of a part of the "negative ions" detected by the positrons in the crystals. We suggest that the annealed defects might be the irradiation-induced "negative ions" rather than the native ones because the annealing temperatures are much lower than the crystal growth temperature using the modified Lely method (>1800 °C). This "negative ions" annealing phenomenon has already been observed by Polity *et al.* [69] in 2-MeV electrons irradiated $6H$-SiC crystals then annealed between 450 °C and 900 °C.

## VIII. COMPARISON WITH PREVIOUS EXPERIMENTAL STUDIES

Our calculated positron lifetimes can be compared to the ones observed experimentally in previous studies. For this comparison we use lifetimes scaled to the experimental lattice lifetime of 140 ps.

Barthe *et al.* [4] observed lifetimes of 257- and 281-ps lifetimes in *n*-type 6*H*-SiC implanted with low-energy protons (after 900 °C and 1300 °C annealing, respectively). These defects were identified as $(V_C + V_{Si})_2$ and $(V_C + V_{Si})_3$. Our calculations confirm this interpretation since we obtained lifetimes of 262 ps for the tetravacancy and 263 and 296 ps for the two configurations of the hexavacancy.

Aavikko *et al.* [70] studied undoped SiC samples annealed at 1600 °C. They observed long-lifetime components of 261, 283, and 284 ps, which were attributed to clusters containing four and five vacancies, respectively. This is consistent with our calculations, as these lifetimes are close to what we obtained for $(V_C + V_{Si})_2$ and $(V_C + V_{Si})_3$. It should be noted, however, that in the case of SiC, the number of silicon vacancies in the cluster has more influence on the positron lifetime than the total number of vacancies.

Finally, Brauer *et al.* [13] studied 6*H*-SiC samples irradiated with 200-keV $Ge^+$ ions, at fluences varying from $10^{16}$ to $10^{19}$ m$^{-2}$. For the lowest fluence, a long-lifetime component of 235 ps was observed and attributed to the divacancy, even though it was longer than what Brauer *et al.* had calculated for this type of defect. The authors indicated that the discrepancy between the measured and calculated lifetimes could come from the fact that the relaxation effects were not taken into account. Our results confirm this, as our calculations yielded 235 ps for the relaxed $V_C + V_{Si}$ cluster. For the $10^{19}$ m$^{-2}$ fluence, Brauer *et al.* observed a lifetime component of 305 ps and attributed it to a defect containing six vacancies. We calculated a lifetime of 296 ps for the ring hexavacancy so this defect could be the one observed in this study.

## IX. CONCLUSIONS

We characterized irradiated and annealed 6*H*-SiC crystals using EPR and PAS. The results were interpreted in the light of our positron and formation energies calculations. The combined characterization methods showed the presence of silicon vacancies in irradiated 6*H*-SiC, which was confirmed by the positron lifetime calculations. During annealing at temperatures starting at around 400 °C–500 °C migration of the silicon vacancies and formation of a larger defect were observed. This defect, exhibiting a positron lifetime of 235 ps, was identified as $V_C + V_{Si}$ based both on the charge state and positron lifetime calculations.

We calculated the positron lifetimes and formation energies for vacancy clusters containing from two to six vacancies. The calculated formation energies enabled us to predict the most stable charge states of the defects. We showed that the atomic relaxation has less influence on the calculated positron lifetimes for vacancy clusters than it does for the monovacancies. However, this effect is not negligible and should be taken into account in the calculations. We also showed that in silicon carbide the positron lifetime is mainly affected by the number of the silicon vacancies in the cluster. Additionally, in the case of the large vacancy clusters, such as hexavacancy, we observed that not only the number of vacancies, but also their configuration strongly affects the positron lifetime.

We compared our calculated results with experimental lifetimes reported in literature. The calculated positron lifetimes enabled us to confirm the identification of vacancy clusters done in previous studies by means of positron annihilation spectroscopy.

[1] P. Yvon and F. Carré, J. Nucl. Mater. **385**, 217 (2009).

[2] L. Giancarli, M. Ferrari, M. A. Fütterer, and S. Malang, Fusion Eng. Des. **49**, 445 (2000).

[3] L. Torpo, T. E. M. Staab, and R. M. Nieminen, Phys. Rev. B **65**, 085202 (2002).

[4] M.-F. Barthe, D. T. Britton, C. Corbel, A. Hempel, L. Henry, P. Desgardin, W. Bauer-Kugelmann, G. Kögel, P. Sperr, and W. Triftshäuser, Physica B **308**, 668 (2001).

[5] G. Brauer, W. Anwand, E.-M. Nicht, J. Kuriplach, M. Šob, N. Wagner, P. G. Coleman, M. J. Puska, and T. Korhonen, Phys. Rev. B **54**, 2512 (1996).

[6] A. Zywietz, J. Furthmüller, and F. Bechstedt, Phys. Rev. B **59**, 15166 (1999).

[7] T. E. M. Staab, L. M. Torpo, M. J. Puska, and R. M. Nieminen, Mater. Sci. Forum **353**, 533 (2000).

[8] L. Torpo, M. Marlo, T. E. M. Staab, and R. M. Nieminen, J. Phys.: Condens. Matter **13**, 6203 (2001).

[9] M. Bockstedte, A. Mattausch, and O. Pankratov, Phys. Rev. B **68**, 205201 (2003).

[10] F. Bruneval and G. Roma, Phys. Rev. B **83**, 144116 (2011).

[11] F. Bruneval, Nucl. Instrum. Methods Phys. Res., Sect. B **277**, 77 (2012).

[12] A. Kawasuso, H. Itoh, S. Okada, and H. Okumura, J. Appl. Phys. **80**, 5639 (1996).

[13] G. Brauer, W. Anwand, P. G. Coleman, A. P. Knights, F. Plazaola, Y. Pacaud, W. Skorupa, J. Störmer, and P. Willutzki, Phys. Rev. B **54**, 3084 (1996).

[14] A. Kawasuso, H. Itoh, N. Morishita, M. Yoshikawa, T. Ohshima, I. Nashiyama, S. Okada, H. Okumura, and S. Yoshida, Appl. Phys. A **67**, 209 (1998).

[15] C. C. Ling, C. D. Beling, and S. Fung, Phys. Rev. B **62**, 8016 (2000).

[16] S. Arpiainen, K. Saarinen, P. Hautojärvi, L. Henry, M.-F. Barthe, and C. Corbel, Phys. Rev. B **66**, 075206 (2002).

[17] L. Henry, M.-F. Barthe, C. Corbel, P. Desgardin, G. Blondiaux, S. Arpiainen, and L. Liszkay, Phys. Rev. B **67**, 115210 (2003).

[18] C. H. Lam, T. W. Lam, C. C. Ling, S. Fung, C. D. Beling, H. De-Sheng, and W. Huimin, J. Phys.: Condens. Matter **16**, 8409 (2004).

[19] H. J. von Bardeleben, J. L. Cantin, L. Henry, and M.-F. Barthe, Phys. Rev. B **62**, 10841 (2000).

[20] N. T. Son, P. N. Hai, and E. Janzén, Phys. Rev. B **63**, 201201 (2001).

[21] X. Kerbiriou, M.-F. Barthe, S. Esnouf, P. Desgardin, G. Blondiaux, and G. Petite, J. Nucl. Mater. **362**, 202 (2007).

[22] J. Lefèvre, J.-M. Costantini, D. Gourier, S. Esnouf, and G. Petite, Phys. Rev. B **83**, 075201 (2011).

[23] P. G. Baranov, A. P. Bundakova, A. A. Soltamova, S. B. Orlinskii, I. V. Borovykh, R. Zondervan, R. Verberk, and J. Schmidt, Phys. Rev. B **83**, 125203 (2011).

[24] N. T. Son, X. T. Trinh, L. S. Løvlie, B. G. Svensson, K. Kawahara, J. Suda, T. Kimoto, T. Umeda, J. Isoya, T. Makino, T. Ohshima, and E. Janzén, Phys. Rev. Lett. **109**, 187603 (2012).

[25] N. T. Son, P. Carlsson, J. ul Hassan, E. Janzén, T. Umeda, J. Isoya, A. Gali, M. Bockstedte, N. Morishita, T. Ohshima, and H. Itoh, Phys. Rev. Lett. **96**, 055501 (2006).

[26] P. Carlsson, N. T. Son, A. Gali, J. Isoya, N. Morishita, T. Ohshima, B. Magnusson, and E. Janzén, Phys. Rev. B **82**, 235203 (2010).

[27] R. M. Nieminen, E. Boroński, and L. J. Lantto, Phys. Rev. B **32**, 1377 (1985).

[28] J. Wiktor, G. Jomard, M. Torrent, and M. Bertolus, Phys. Rev. B **87**, 235207 (2013).

[29] M. Saito and A. Oshiyama, Phys. Rev. B **53**, 7810 (1996).

[30] I. Makkonen, M. Hakala, and M. J. Puska, Phys. Rev. B **73**, 035103 (2006).

[31] I. Makkonen and M. J. Puska, Phys. Rev. B **76**, 054119 (2007).

[32] F. Tuomisto and I. Makkonen, Rev. Mod. Phys. **85**, 1583 (2013).

[33] http://www.srim.org/SRIM/SRIMINTRO.htm

[34] R. Krause-Rehberg and H. S. Leipner, *Positron Annihilation in Semiconductors: Defect Studies*, Vol. 127 (Springer, Berlin, 1999).

[35] C. Corbel, M. Stucky, P. Hautojärvi, K. Saarinen, and P. Moser, Phys. Rev. B **38**, 8192 (1988).

[36] P. Kirkegaard and M. Eldrup, Comput. Phys. Commun. **3**, 240 (1972).

[37] M. J. Puska and R. M. Nieminen, Rev. Mod. Phys. **66**, 841 (1994).

[38] S. B. Zhang and J. E. Northrup, Phys. Rev. Lett. **67**, 2339 (1991).

[39] M. Leslie and N. J. Gillan, J. Phys. C: Solid State Phys. **18**, 973 (1985).

[40] S. Lany and A. Zunger, Modell. Simul. Mater. Sci. Eng. **17**, 084002 (2009).

[41] S. E. Taylor and F. Bruneval, Phys. Rev. B **84**, 075155 (2011).

[42] Y. Goldberg, in *Properties of Advanced Semiconductor Materials GaN, AlN, InN, BN, SiC, SiGe*, edited by M. E. Levinshtein, S. L. Rumyantsev, and M. S. Shur (Wiley, New York, 2001).

[43] L. Gilgien, G. Galli, F. Gygi, and R. Car, Phys. Rev. Lett. **72**, 3214 (1994).

[44] E. Boroński and R. M. Nieminen, Phys. Rev. B **34**, 3820 (1986).

[45] M. J. Puska, A. P. Seitsonen, and R. M. Nieminen, Phys. Rev. B **52**, 10947 (1995).

[46] M. Torrent, F. Jollet, F. Bottin, G. Zérah, and X. Gonze, Comput. Mater. Sci. **42**, 337 (2008).

[47] X. Gonze, G.-M. Rignanese, M. Verstraete, J.-M. Beuken, Y. Pouillon, R. Caracas, F. Jollet, M. Torrent, G. Zérah, M. Mikami, P. Ghosez, M. Veithen, J.-Y. Raty, V. Olevano, F. Bruneval, L. Reining, R. Godby, G. Onida, D. R. Hamann, and D. C. Allan, Z. Kristallogr. **220**, 558 (2005).

[48] X. Gonze, J.-M. Beuken, R. Caracas, F. Detraux, M. Fuchs, G.-M. Rignanese, L. Sindic, M. Verstraete, G. Zérah, F. Jollet, M. Torrent, A. Roy, M. Mikami, P. Ghosez, J.-Y. Raty, and D. C. Allan, Comput. Mater. Sci. **25**, 478 (2002).

[49] X. Gonze, B. Amadon, P.-M. Anglade, J.-M. Beuken, F. Bottin, P. Boulanger, F. Bruneval, D. Caliste, R. Caracas, M. Côté, T. Deutsch, L. Genovese, P. Ghosez, M. Giantomassi, S. Goedecker, D. R. Hamann, P. Hermet, F. Jollet, G. Jomard, S. Leroux, M. Mancini, S. Mazevet, M. J. T. Oliveira, G. Onida, Y. Pouillon, T. Rangel, G.-M. Rignanese, D. Sangalli, R. Shaltaf, M. Torrent, M. J. Verstraete, G. Zerah, and J. W. Zwanziger, Comput. Phys. Commun. **180**, 2582 (2009).

[50] N. A. W. Holzwarth, A. R. Tackett, and G. E. Matthews, Comput. Phys. Commun. **135**, 329 (2001).

[51] C. G. Broyden, J. Inst. Math. Appl. **6**, 221 (1970).

[52] R. Fletcher, Comput. J. **13**, 317 (1970).

[53] D. Goldfarb, Math. Comput. **24**, 23 (1970).

[54] D. F. Shanno, Math. Comput. **24**, 647 (1970).

[55] J. P. Perdew, K. Burke, and M. Ernzerhof, Phys. Rev. Lett. **77**, 3865 (1996).

[56] L. Patrick and W. J. Choyke, Phys. Rev. B **2**, 2255 (1970).

[57] N. Mizuochi, S. Yamasaki, H. Takizawa, N. Morishita, T. Ohshima, H. Itoh, and J. Isoya, Phys. Rev. B **66**, 235202 (2002).

[58] S. B. Orlinski, J. Schmidt, E. N. Mokhov, and P. G. Baranov, Phys. Rev. B **67**, 125207 (2003).

[59] E. Sörman, N. T. Son, W. M. Chen, O. Kordina, C. Hallin, and E. Janzén, Phys. Rev. B **61**, 2613 (2000).

[60] N. Mizuochi, S. Yamasaki, H. Takizawa, N. Morishita, T. Ohshima, H. Itoh, T. Umeda, and J. Isoya, Phys. Rev. B **72**, 235208 (2005).

[61] L. Torpo, R. Nieminen, K. Laasonen, and S. Poykko, Appl. Phys. Lett. **74**, 221 (1999).

[62] T. Wimbauer, B. K. Meyer, A. Hofstaetter, A. Scharmann, and H. Overhof, Phys. Rev. B **56**, 7384 (1997).

[63] T. E. M. Staab, M. Haugk, T. Frauenheim, and H. S. Leipner, Phys. Rev. Lett. **83**, 5519 (1999).

[64] D. V. Makhov and L. J. Lewis, Phys. Rev. Lett. **92**, 255504 (2004).

[65] J. Wiktor, G. Jomard, and M. Bertolus, Nucl. Instrum. Meth. B **327**, 63 (2014).

[66] A. Kokalj, J. Mol. Graphics Modell. **17**, 176 (1999).

[67] A. Kokalj, Comput. Mater. Sci. **28**, 155 (2003).

[68] Z. Zolnai, N. Son, C. Hallin, and E. Janzén, J. Appl. Phys. **96**, 2406 (2004).

[69] A. Polity, S. Huth, and M. Lausmann, Phys. Rev. B **59**, 10603 (1999).

[70] R. Aavikko, K. Saarinen, F. Tuomisto, B. Magnusson, N. T. Son, and E. Janzén, Phys. Rev. B **75**, 085208 (2007).